Astron. Astrophys. 350, 447–456 (1999)

ASTRONOMY AND ASTROPHYSICS

Polarimetric structure in the first Galactic quadrant from the 2.695 GHz Effelsberg survey

A.R. Duncan, P. Reich, W. Reich, and E. Fürst

Max-Planck-Institut für Radioastronomie, Auf dem Hügel 69, 53121 Bonn, Germany

Received 26 May 1999 / Accepted 19 July 1999

Abstract. Polarimetric data from the 2.695 GHz Effelsberg survey of the Galactic Plane have been reduced, resulting in images of the Stokes Q and U emission components over Galactic longitudes given by $74^\circ \geq l \geq 4\overset{\circ}{.}9$, at a resolution of $4\overset{\prime}{.}3$. This extends the earlier work of Junkes et al. (1987a) out to the latitude limit of the survey observations ($b = \pm 5^\circ$). Patchy, diffuse polarised emission is seen to extend to high latitudes ($|b| = 5^\circ$), with generally brighter polarisation detected above $|b| \gtrsim 2^\circ$. The distributions of both the polarised intensities and polarisation position-angles are shown, as a function of Galactic longitude, and compared with similar data from the southern Galactic Plane. These data will assist in higher resolution studies of the Galactic magnetic field and the magneto-ionic properties of the interstellar medium.

Between longitudes of $20^\circ - 45^\circ$, bright patches of polarised emission are detected, which exhibit quasi-periodic variations of the polarisation angles with scale-sizes of approximately 7°. Both the characteristics and the possible origins of these structures are discussed. This bright emission appears to originate from the Sagittarius spiral arm, between distances of approximately 2.5 and 8 kpc. An anticorrelation between polarised intensities and regions of enhanced H I gas density (lying at kinematic distances of 2–2.5 kpc) is found. Possible mechanisms are suggested to account for this anticorrelation, arising through the action of a Faraday "screen" associated with the Sagittarius arm.

The structured, quasi-periodic nature of the polarisation position-angles over this region of the Plane most likely results from a peculiar magnetic field geometry associated with the Sagittarius arm. With scale-sizes of between 200 and 600 pc, such magnetic field geometries may be produced by a mechanism similar to the Parker instability.

Key words: techniques: polarimetric – surveys – ISM: magnetic fields – Galaxy: general – radio continuum: general

1. Introduction

The results of a sensitive, radio continuum survey of the Galactic Plane were presented by Reich et al. (1984). This survey, observed with the 100-m Effelsberg radio telescope at a frequency of 2.695 GHz, combined a high resolution, good sensitivity and polarimetric capabilities, and covered almost 80° of Galactic longitude. Specifically, this work examined Galactic longitudes of $76^\circ \geq l \geq 357\overset{\circ}{.}4$, with a latitude range of $|b| \leq 1\overset{\circ}{.}5$.

In addition to the total-power work presented by Reich et al. (1984), maps of the linearly polarised emission with a resolution of $4\overset{\prime}{.}3$ were analyzed and presented by Junkes et al. (1987a, 1987b). It was this work which first revealed the presence of diffuse polarised emission on small angular scales, and that this emission was distributed in a "patchy" manner (see also Wieringa et al. 1993). It is important to note that the Junkes et al. work was restricted to a latitude range of $|b| \leq 1\overset{\circ}{.}5$.

Over the next few years, as interpretation of this original polarimetric data continued (see Junkes et al. 1990), the Effelsberg 2.695 GHz survey also progressed. Reich et al. (1990b) presented total-power maps of the radio emission over longitudes of $76^\circ \geq l \geq -2^\circ$ (approximately the same longitude range as the Reich et al. 1984 work), but with a latitude coverage of $|b| \leq 5^\circ$. Fürst et al. (1990) extended the longitude coverage further still, so that the total-power survey now images $240^\circ \geq l \geq -2^\circ$ in longitude, and out to $\pm 5^\circ$ in latitude. No more polarimetric data were reduced, however.

2. Recent Parkes work

The 64-m Parkes radio telescope has been used to undertake a similar, polarimetric survey of the southern Galactic Plane at a frequency of 2.4 GHz (see Duncan et al. 1995, 1997), with a resolution of $10\overset{\prime}{.}4$. As part of this latter work, the polarimetric data were reduced over the entire survey area (spanning longitudes of $5^\circ \geq l \geq 238^\circ$), producing images of the polarised intensity and polarisation position angle out to the latitude limit of the survey ($b = \pm 5^\circ$, although over some regions this has been extended to $b = +7^\circ$ and $b = -8^\circ$).

The Parkes observations revealed the same faint, diffuse polarised emission as had been detected by Junkes et al. (1987a).This polarisation was also seen to have a very mottled and "patchy" distribution. However, the Parkes survey showed this faint and patchy emission to continue out to the latitude limit of the survey (and presumably beyond). Furthermore, the Parkes data provide evidence that a large component of this

Send offprint requests to: W. Reich

Table 1. Receiver data, telescope parameters and assumed calibrator values for the Effelsberg survey. The rms noise and brightness sensitivity information are given for the $5\farcm1$ resolution images. The $T_b\ S^{-1}$ value is also quoted for $5\farcm1$ angular resolution. The uncertainty in the polarisation position-angle is given as a function of the polarised intensity PI (mJy/b.a.).

Centre frequency	2.695 GHz
Receiver bandwidth	50–80 MHz
System temperature	60 K
Beamwidth (HPBW)	$4\farcm3 \pm 0\farcm1$
Map resolution (HPBW)	$5\farcm1 \pm 0\farcm1$
Q and U RMS Noise	2.5 mJy/b.a.
Q and U RMS brightness temperature	9 mK
PI RMS Noise	3.0 mJy/b.a.
PI RMS brightness temperature	11 mK
$T_b\ S^{-1}$	3.58 K/Jy
Position angle error (degrees)	$\left(4 + \frac{5\times10^3}{PI^2}\right)^{0.5}$
Scan interval and pixel spacing	$2\farcm0$
3C286 assumed flux density	(10.4 ± 0.1) Jy
3C286 fractional polarisation	(9.9 ± 0.2)%
3C286 position angle	$(33 \pm 2)^\circ$

faint, mottled emission is distributed over the southern Plane in a quasi-uniform manner.

These new and interesting results, emerging from the higher latitude Plane emission, have prompted a re-examination of the 2.695 GHz Effelsberg data. Specifically, we have applied the data reduction software and techniques developed for the Parkes survey to the higher latitude Effelsberg polarisation data ($1\fdg5 \leq |b| \leq 5\fdg0$). These data are combined with the lower latitude data of Junkes et al. (1987a), producing polarimetric images out to latitudes of $b = \pm5^\circ$. The longitude range examined is $74^\circ \geq l \geq 4\fdg9$, similar to that of Junkes et al. (1987a).

3. The Effelsberg observations

Here, we are reducing data from the 100-m Effelsberg telescope, observed by both Reich et al. (1984) and Reich et al. (1990b). The equipment, observing and calibration procedures are described in some detail in both Reich et al. (1984) and Junkes et al. (1987a). Some of the telescope and observing parameters are listed in Table 1.

The receiver used was a 3 channel, cooled FET (field effect transistor) based device. Coupled with the polarimeter (Reich et al. 1984), this arrangement produced data for the Stokes parameters I, Q and U.

The Effelsberg radio telescope itself is a large and fully steerable parabolic dish, 100 m in diameter, on an alt-azimuth mounting. The observations were made by scanning the telescope in directions of Galactic longitude (l-scans) and Galactic latitude (b-scans), at a rate of 2° per minute in the coordinate system. A separation of $2'$ was used between adjacent scans and adjacent pixels, as this provided fully sampled data (i.e. more than 2 points per HPBW). Each scan was typically 3° in length. Because of this, the area to be observed was built up as a series of smaller regions, each of which was approximately $3^\circ \times 3^\circ$ in extent.

Calibration of the data was performed by scaling the observations against the bright, point-like source 3C286 (see Table 1). The flux density of this source is taken from Baars et al. (1977), and the polarimetric characteristics from Tabara & Inoue (1980).

4. Data reduction

The longitudes examined here lie between $4\fdg9 \leq l \leq 74\fdg0$, and the latitudes between $1\fdg5 \leq |b| \leq 5\fdg0$. This longitude range was divided into 4 "blocks", each of which was approximately 20° in length. The preliminary data reduction was performed using standard software, based on the NOD2 reduction system (Haslam 1974).

At this point the scans had been assembled into several hundred crude maps, each of which was of the order of $3^\circ \times 3^\circ$ in size and which had been appropriately calibrated. These maps were then sorted and assembled into both l- and b-scanned maps (l-maps and b-maps) of all 4 blocks. Each of the blocks was examined for interference, bad data points or baseline problems; any affected areas were either corrected or flagged.

During the assembling process, it was carefully checked that no baseline discontinuities existed near the boundaries of each of the small maps. If a discontinuity was detected, the baseline was corrected by the subtraction of an appropriate baselevel from the scan. For Stokes Q and U data, these baselevels were determined by fitting a zeroth- or first-order polynomial function to the scan data, and subtracting this fit. This is equivalent to requiring that the sum of all pixel values in the scan is equal to zero (and also, in the case of a first-order fit, that there is no linear slope along the length of the scan). Whilst the requirement that the sum of pixel values equates to zero will never be exactly satisfied in practice, this condition is met to a good approximation in this instance. (Indeed, this is usually an acceptable approximation whenever the scan length is appreciably greater than the largest structures present in the data.)

Next, the baselevels of each column in the b-maps (10° in length) and each row in the l-maps (approximately 20° in length) were adjusted, by using a similar "cross baselining" procedure to that described by Duncan et al. (1995). Briefly, this process involves subtracting each scan in each l-map (b-map) from its corresponding b-map (l-map) pixels, and fitting a low-order polynomial (third order or less) to the residual. Any points differing from the fit by more than 5σ were flagged as being associated with sources, and the fit repeated. This second fit was then subtracted from the scan. Such a two-pass approach to the polynomial fitting greatly improved the fit quality in the vicinity of bright sources, which exhibit significant amounts of instrumental polarisation.

4.1. Instrumental polarisation

The instrumentally polarised component of the emission was estimated by Junkes et al. (1987a) to be approximately 0.7%. As with the Parkes 2.4 GHz survey data (Duncan et al. 1997),

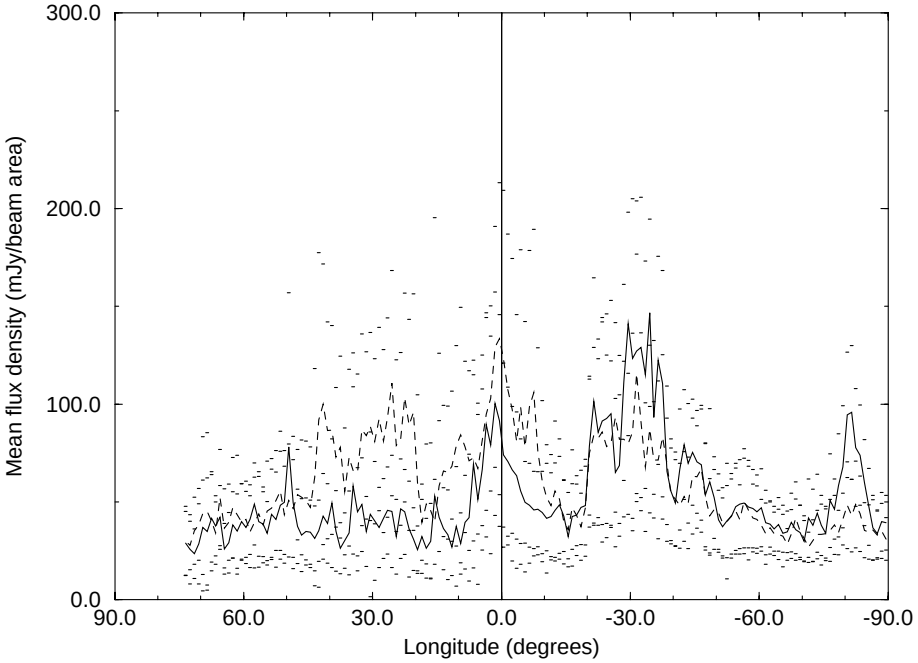

Fig. 1. Mean polarised intensity values over the Galactic Plane, binned into 1° intervals of longitude. Data for $l > 5^\circ$ are from the Effelsberg 2.695 GHz survey, and data with $l < 5^\circ$ are from the Parkes 2.4 GHz survey. The dashed line shows the mean values of points with $|b| \geq 2^\circ$; the solid line for points with $|b| \leq 2^\circ$. The small dashes seen across the figure indicate the standard deviation of each point (these are placed at both $\pm 1\sigma$), and hence provide a measure of the uniformity of the polarised intensities in each bin.

the instrumental component was detected only in the vicinity of bright, discrete sources, usually appearing in the Stokes Q and U images with the distinctive quadrupole pattern.

Examination of the images revealed that only sources with flux densities exceeding some tens of Jy per beam area produced prominent instrumental polarisation. The strongest such sources appearing in the data can be identified with H II regions such as W31, W33, M17, W43 and W51. As in the Junkes et al. (1987a) work, we have chosen not to remove this instrumental component.

4.2. Combining

Each pair of l- and b-scanned maps was then combined, using the "Plait" software of Emerson & Gräve (1988). Note that, over some isolated regions of the data, we could not obtain both l- and b-scanned observations. Over these areas, some scanning effects may be evident.

The overlap regions of adjacent blocks were examined and it was confirmed that no discontinuities existed at block boundaries; hence, no extra baselevels were added. All the blocks were then combined to form the survey "strip".

At this point, the data were combined with the existing, low-latitude maps of Junkes et al. (1987a). Note that these latter maps consisted of b-scans only. Discontinuities between the low- and high-latitude regions were removed as much as possible, although some isolated regions of discontinuity are still evident.

To improve the signal to noise ratio, both the Stokes Q and the Stokes U surveys were then smoothed with a Gaussian which increased the effective beamwidth to 1.2 times the nominal telescope beamwidth (to $5\farcm1$; see Table 1) and appropriately rescaled.

The final polarised intensity images were then formed from the corresponding Stokes Q and U data, in the usual manner. Bias in the polarised intensity images was removed to first order (Wardle & Kronberg 1974; Killeen et al. 1986).

5. Results and discussion

The data reduction process resulted in high-quality images of the Stokes Q and U emission, over much of the first Galactic quadrant. In addition to being shown herein (Figs. 3–5), these data are all available on-line; see the end of the paper for details.

It should be noted, however, that the observing technique (using scan lengths of approximately 3°), as well as the reduction procedures applied to the data, attenuate structure on scale-sizes of the order of 5° and larger. Hence, it must be stressed that Stokes Q and U emission components on these (and larger) angular scales will not be correctly represented in the survey data.

Note that the intensity calibration of the high-latitude data ($|b| \geq 1\fdg5$) is accurate to approximately 5%.

5.1. Distribution of polarised intensities

The distribution of polarised intensities in the first and fourth Galactic quadrants is shown in Fig. 1. This (and Fig. 2) contain data from the Effelsberg survey for Galactic longitudes greater than 5°, and the Parkes survey (Duncan et al. 1997) for longitudes less than 5°. Before plotting, the Effelsberg data were convolved to the beam size of the Parkes survey ($10\farcm4$), and regridded to match the pixel size and spacing of the Parkes images ($4\farcm0$).

Examination of Fig. 1 reveals a general symmetry in the polarised intensity distribution in the first and fourth Galactic quadrants. First, bright emission is seen at both low and high lat-

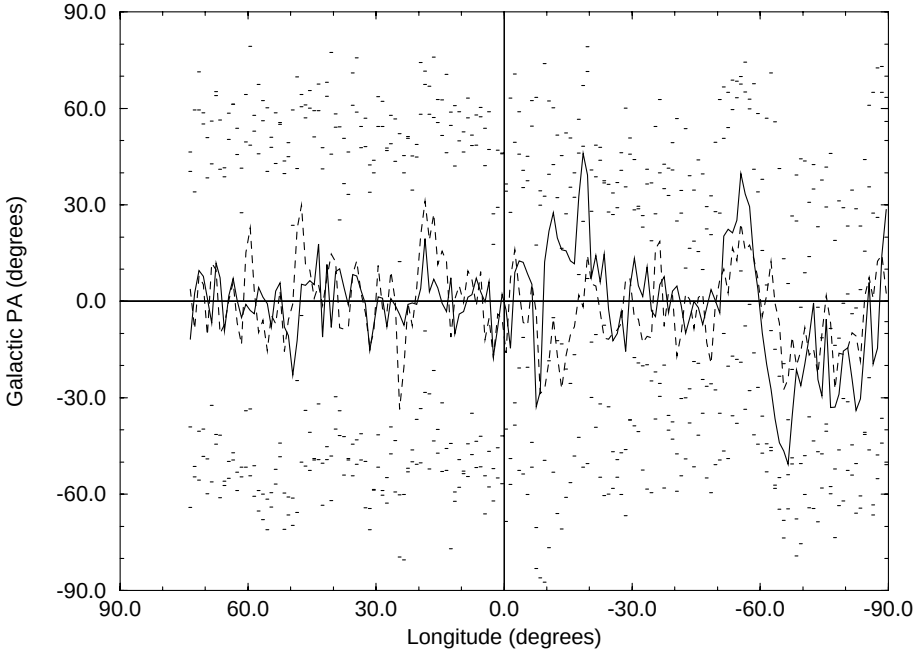

Fig. 2. The distribution of polarisation position-angles along the Galactic Plane, binned into 1° intervals of longitude, showing the orientation of the electric vector of the received radiation. Data for $l > 5^\circ$ are from the Effelsberg 2.695 GHz survey, and data with $l < 5^\circ$ are from the Parkes 2.4 GHz survey. The dashed line shows the mean values of points with $|b| \geq 2^\circ$; the solid line for points with $|b| \leq 2^\circ$. A vector of angle 0° is oriented perpendicular to the Galactic Plane, and rotates anti-clockwise as the angle increases. The small dashes scattered across the figure indicate the standard deviation of each bin (these are placed at both $\pm 1\sigma$).

itudes, around the Galactic Centre (GC). This is predominantly due to the presence of a bright "plume" of polarised emission in this region, detected by the 2.4 GHz Parkes survey (Duncan et al. 1998). The Effelsberg data confirm that this plume extends no further than approximately 5° into the first Galactic quadrant.

Second, bright, large-scale polarisation is seen in both the northern and southern sections of the Plane, at distances from the GC of between 20° and 45°. It should be noted, however, that the characteristics of these two regions appear quite different. In the south, the low and high latitude data are comparable, but with slightly higher values closer to the Plane. By contrast, the northern region is somewhat fainter overall, and is present in the high latitude curve alone. Hence, the polarisation enhancements are less dependent on latitude (i.e. more diffuse) in the south, but show a strong concentration to $|b| > 2^\circ$ in the north. The polarised intensity distribution associated with this northern enhancement will be further discussed in Sect. 5.4.

Third, about $\pm 50^\circ$ from the GC, both the low and high latitude curves tend towards minima of approximately 30 mJy beam area^{-1} (with the exception of a low latitude "bump" near -80° longitude). The standard deviations are also smallest in these regions. Although not shown, the southern data continue this trend to a longitude of -122° (the edge of the survey), prompting the idea that this represents a quasi-uniform "background" level of polarised emission (Duncan et al. 1997). The addition of the Effelsberg data, which exhibits similar minima, supports this hypothesis.

5.2. Distribution of polarisation position angles

The distribution of polarisation position-angles in the first and fourth Galactic quadrants is shown in Fig. 2. As in Fig. 1, the data are averaged into 1° intervals of Galactic longitude.

Considering Fig. 2, it can be seen that the data on either side of the GC exhibit very different characteristics. Whilst southern longitudes contain several areas of large-scale structure in the position-angles, such regions are essentially absent from northern longitudes. Furthermore, the distribution of standard deviations is much more uniform over positive longitudes. This suggests that, on scale-sizes of degrees, the polarisation position-angles from the Effelsberg survey ($l > 5^\circ$) are more random and uncorrelated than those from the Parkes survey ($l < 5^\circ$).

5.3. Differences between the Effelsberg and Parkes surveys

The data presented in Figs. 1 and 2 (and particularly that in Fig. 2) indicate significant differences between the Effelsberg and Parkes surveys. In particular, the Effelsberg survey appears less sensitive to the largest scale-sizes of structure than does its southern counterpart (scale-sizes of the order of $5^\circ - 10^\circ$).

To confirm this interpretation, large-scale structure was approximately subtracted from the Stokes Q and U images for longitudes of $l < 5^\circ$. The subtraction was performed using the method of "unsharp masking", as used by Sofue & Reich (1979). Structure on angular scales $\approx 4^\circ$ and larger was subtracted from the Parkes images. Polarised-intensity and polarisation position-angle maps were then generated from the Q and U components.

The filtered Parkes data displayed characteristics much more like those of the Effelsberg survey. Specifically, large-scale structures in the position-angle data were removed, and the standard deviations appeared much more uniform. Interestingly, almost all of the large-scale polarised-intensity structure remained unchanged. This is also consistent with the observations, because the "minimum" polarised intensity (approximately 30 mJy beam area^{-1}), as seen in Fig. 1, is similar in both the Effelsberg and Parkes data.

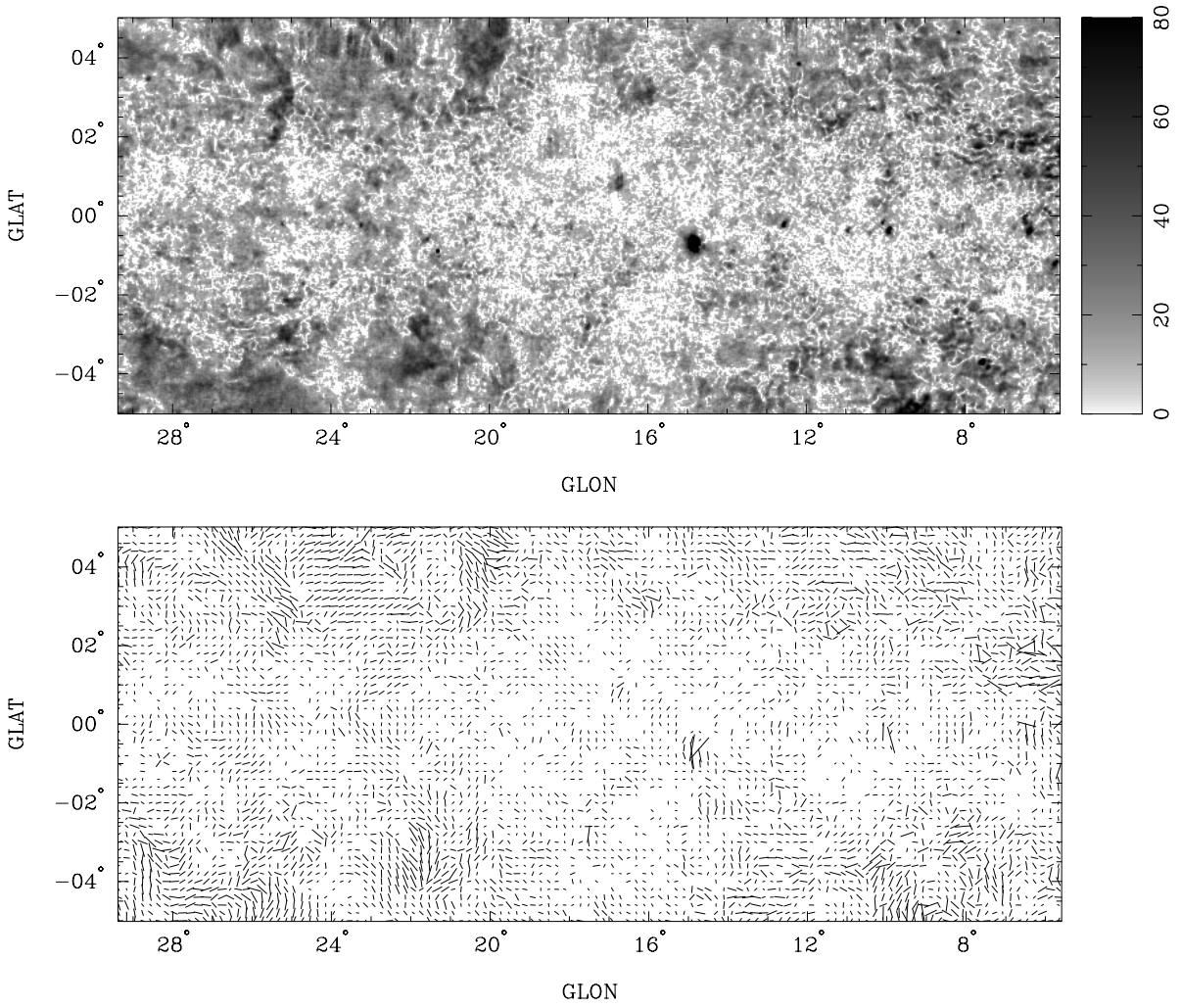

Fig. 3. **a** A grey-scale image detailing the polarised intensities over the longitude range $28^\circ \geq l \geq 4\overset{\circ}{.}9$. The rms noise is approximately 2 mJy beam area^{-1}, with a resolution of $5\overset{\prime}{.}1$. The grey-scale wedge is labelled in units of mJy beam area^{-1}. **b** Polarisation position-angles over the same region, showing the orientation of the electric vector of the received radiation. The length of each vector is proportional to the intensity of the polarised emission at each point, with a maximum polarised intensity of 880 mJy beam area^{-1}. The vector lengths are clipped at 100 mJy beam area^{-1}. Data are blanked wherever the intensity falls below 2σ. A vector is plotted every $12'$.

The differences between the Effelsberg and Parkes surveys, discussed above, result primarily from the differences in observing procedure. As noted in Sect. 3, the Effelsberg observations used scan lengths of typically 3°. In contrast, the Parkes survey employed scan lengths of between 10° and 20°. It is because of these longer scans that the data reduction procedure is able to retain more of the large angular-scale emission and structure.

5.4. Bright polarisation near 30° *longitude*

In Fig. 1, bright, polarised emission can be seen at $|b| \gtrsim 2^\circ$, between longitudes of approximately 20° and 45°. The polarised-intensity images of this region of the Plane appear in Figs. 3a and 4a, and the polarisation position-angle maps are shown in Figs. 3b and 4b. Note that the position-angle map shows the electric vector of the received radiation.

The bright emission seen in this region at latitudes $|b| \gtrsim 2^\circ$ reaches a maximum intensity of approximately 75 mJy beam area^{-1} near $l = 30\overset{\circ}{.}5$, $b = -2\overset{\circ}{.}0$. Most of this high-latitude emission appears as a series of large patches. As with polarisation structure seen in other regions of the Plane, the vector orientations are distinctly "cellular", over angular scales of the order of 2°. Within these cells, the vectors are generally aligned well with each other (indicating that differential Faraday rotation is small over these areas), with regions of depolarisation at cell boundaries. In some areas, the vectors are seen to lie approximately perpendicular to filamentary structures (e.g. the bright filament near $l = 43^\circ, b = -4^\circ$), indicating both that the rotation measures (RMs) produce negligible differential rotation across these features (less than 30 rad m^{-2}), and that coherent magnetic fields exist within the regions.

Fig. 6 shows the distribution of polarisation angles for latitude ranges of both $-5^\circ \leq b \leq -2^\circ$ and $2^\circ \leq b \leq 5^\circ$. As

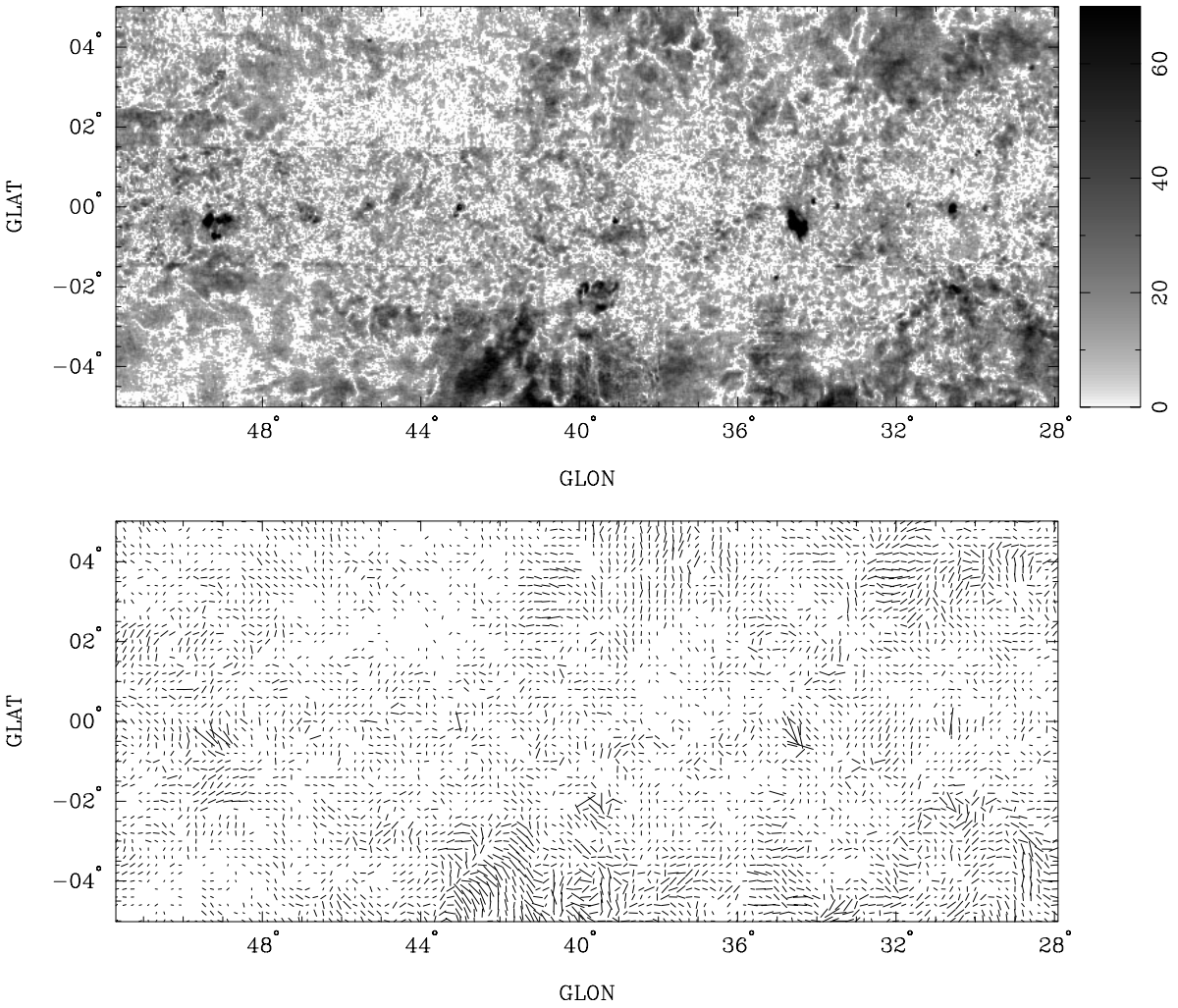

Fig. 4. **a** A grey-scale image detailing the polarised intensities over the longitude range $51^\circ \geq l \geq 27.^\circ 9$. The rms noise is approximately 2 mJy beam area^{-1}, with a resolution of $5.'1$. The grey-scale wedge is labelled in units of mJy beam area^{-1}. **b** Polarisation position-angles over the same region, showing the orientation of the electric vector of the received radiation. The length of each vector is proportional to the intensity of the polarised emission at each point, with a maximum polarised intensity of 680 mJy beam area^{-1}. The vector lengths are clipped at 100 mJy beam area^{-1}. Data are blanked wherever the intensity falls below 2σ. A vector is plotted every $12'$.

in Figs. 1 and 2, the data are binned into longitude intervals of 1°. The peaks in these graphs are fairly regularly spaced, with separations of between 6° and 8°. Fig. 6 clearly shows the presence of coherent, quasi-periodic structure over several tens of degrees of longitude. It is interesting to speculate as to the origins of this structure. Whilst data from the Parkes southern survey also shows evidence of large-scale features in the polarisation position-angle data, no similar quasi-periodic structure has been found.

As mentioned in Sect. 5.1, the large and brightly polarised regions are almost entirely restricted to longitude ranges of between 20° and 45° from the GC, over both positive and negative longitudes (see Fig. 1). This implies that a relationship between Galactic structure and the presence of the brightly polarised regions may exist. Indeed, longitudes of 20° to 45° are coincident with the Sagittarius spiral arm, and -20° to -40° with the Carina arm (Beuermann et al. 1985; Vallée 1997). This highlights the possibility that we are detecting polarised radio emission from these spiral arms. Between longitudes of 20° and 45°, the line of sight through the Sagittarius arm is quite long, starting at approximately 2 kpc and continuing to approximately 8 kpc (Beuermann et al. 1985, assuming a distance from the Sun to the GC of 8.5 kpc).

5.4.1. Anticorrelation with H I data

The possibility of detecting polarised emission from distant spiral arms, and the quasi-periodic nature of the polarisation angles seen in Fig. 6 prompted the examination of H I data (Hartmann & Burton 1997) over this section of the Plane, as this could provide distance information.

Fig. 7 shows both the H I emission and polarised intensity over a section of the Plane. Data below $|b| = 2^\circ$ show very intense H I emission (greatly exceeding the dynamic range of

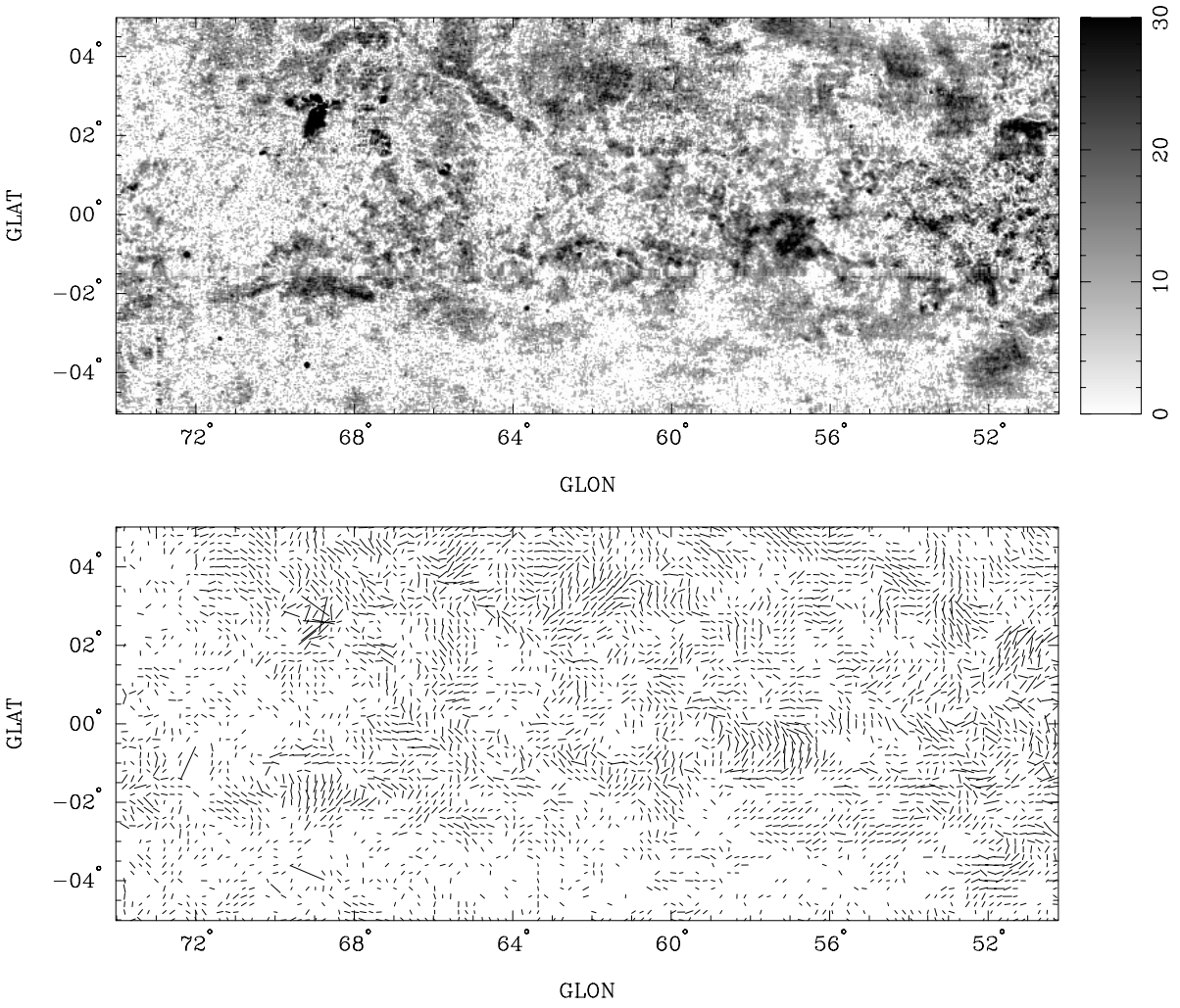

Fig. 5. **a** A grey-scale image detailing the polarised intensities over the longitude range $74^\circ \geq l \geq 50.^\circ 9$. The rms noise is approximately 2 mJy beam area^{-1}, with a resolution of $5.'1$. The grey-scale wedge is labelled in units of mJy beam area^{-1}. **b** Polarisation position-angles over the same region, showing the orientation of the electric vector of the received radiation. The length of each vector is proportional to the intensity of the polarised emission at each point, with a maximum polarised intensity of 200 mJy beam area^{-1}. The vector lengths are clipped at 75 mJy beam area^{-1}. Data are blanked wherever the intensity falls below 2σ. A vector is plotted every $12'$.

the figure), and no polarised emission. The lack of polarisation here is not unexpected, because the increase in thermal electron density and the more turbulent field near $b = 0^\circ$ will produce strong depolarisation. Indeed, this trend can be seen throughout much of the data presented in Figs. 3–5.

However, examining the distribution of polarised intensities in Fig. 7 for $|b| \gtrsim 2^\circ$, a clear tendency for regions of polarised emission to be anticorrelated with regions of bright H I emission is also seen. The velocity ranges over which this is evident are from +25 to +40 km s^{-1} between longitudes of approximately $35^\circ \gtrsim l \gtrsim 20^\circ$, and +35 to +50 km s^{-1} between longitudes of $45^\circ \gtrsim l \gtrsim 35^\circ$. This is consistent with the H I emission originating at kinematic distances of between 1.8 and 2.5 kpc (Brand & Blitz 1993). We again note that the Sagittarius spiral arm is located at distances of between approximately 2 kpc and 8 kpc over these longitudes.

The anticorrelation can arise through two principal means. First, if the polarised radio emission is produced at the same distances as the H I regions (1.8–2.5 kpc), then the polarised emission must be suppressed in regions of dense H I by internal depolarisation effects (Sokoloff et al. 1998). Second, the majority of the polarised emission may be produced at distances greater than those of the H I regions (i.e. between distances of 2.5 and 8 kpc), and then depolarised on its passage through these regions of denser H I by external Faraday dispersion (Sokoloff et al. 1998).

5.4.2. A Faraday “screen” in the Sagittarius spiral arm

If the polarisation detected over this region of the Plane were due to an increase in the intensity of the synchrotron emission, we would expect increases in the polarised emission to correlate with increases in the total-power flux. Specifically, the polarised

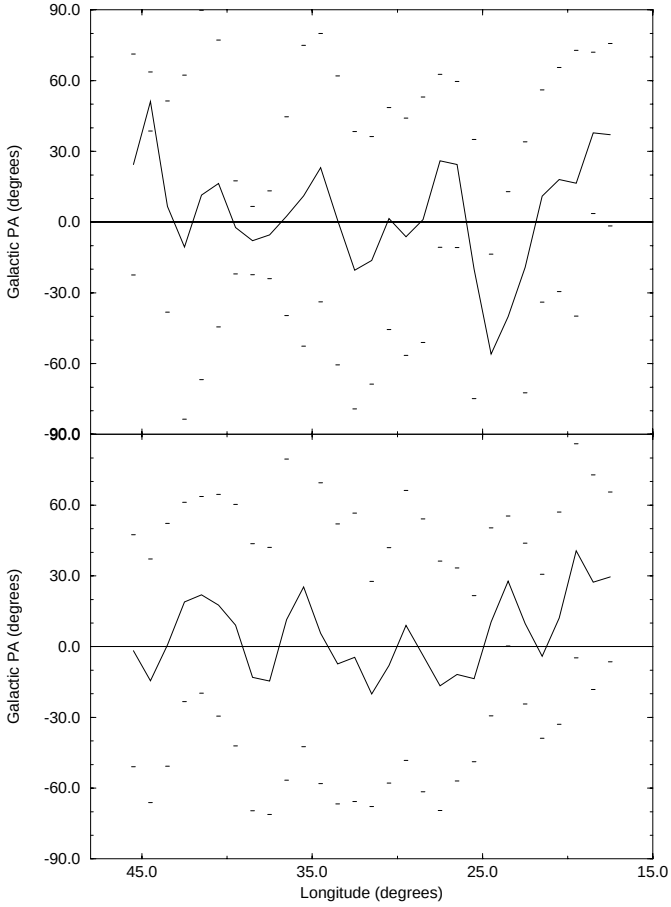

Fig. 6. The distributions of mean polarisation angles over the latitude ranges of $5^\circ \geq b \geq 2^\circ$ (upper graph) and $-5^\circ \leq b \leq -2^\circ$ (lower graph) are shown. As in Fig. 2, the angles have been binned into 1° intervals of longitude, and show the orientation of the electric vector of the received radiation. A vector of angle 0° is oriented perpendicular to the Galactic Plane, and rotates anti-clockwise as the angle increases. The small dashes scattered across the figure indicate the standard deviation of each bin, and are placed at both $\pm 1\sigma$. The peaks in the curves show separations of between 6° and 8°.

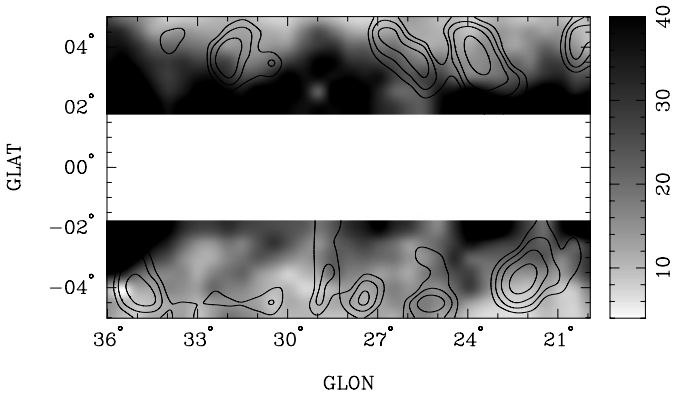

Fig. 7. A grey scale image of the H I gas over a section of the Plane examined in Fig. 6, averaged over a velocity interval of +30 to +39 km s^{-1}. The contours are those of polarised intensity, obtained from Figs. 3 and 4. Before plotting, the distribution of polarised emission was appropriately smoothed to a resolution of 1°, so as to better match the resolution of the H I data. Note the anticorrelation between regions of bright polarised emission, and those of enhanced H I. Data below latitudes of $b = \pm 2^\circ$ have been blanked. The H I intensities towards negative latitudes have been multiplied by 2. Contour levels are: 1.7, 2.3, 3 and 4 Jy beam area^{-1}. The grey scale wedge is labelled in K.

patches should have counterparts in total-power of at least 1.4 times the intensity. However, examination of total-power structure on the same angular scales shows no correlation with polarised intensity. This is also true of the emission on smaller angular scales (as shown in Figs. 3 and 4). Thus, we suggest that the detected anticorrelation is the result of the Faraday depolarisation of more distant polarised emission by a "Faraday screen", which is correlated with the H I discussed before, rather than the result of increases in the synchrotron emissivity. Note that the existence of such screens has been suggested by several other authors, working with interferometric telescope data. Specifically, Wieringa et al. (1993) deduced the presence of a local ($d \lesssim 400$ pc) Faraday-rotating screen from their work at 325 MHz. Similarly, Gray et al. (1999) find evidence for a Faraday screen in a region of the Perseus spiral arm.

From the anticorrelation with H I over the velocity ranges noted above, it is probable that this depolarising "screen" is located on the near side of the Sagittarius spiral arm, at distances of between 1.8 and 2.5 kpc.

The polarised emission upon which the depolarising screen acts cannot originate from more than a few kpc behind the screen. This is because more distant emission is depolarised by differential Faraday rotation within the spiral arm (Sokoloff et al. 1998; Burn 1966).

5.4.3. Sources of the anticorrelation with H I

It is of interest to consider whether H I-associated H II may be the cause of the general anticorrelation seen in Fig. 7. That is, are the areas coincident with bright H I emission depolarised because of a greater density of thermal electrons associated with the brighter regions of H I.

Observations by Reynolds et al. (1995) of a number of H I complexes towards medium and high Galactic latitudes detected thermal particles with column densities of the order of 3×10^{19} cm^{-2} or less. Much of the H I seen in Fig. 7 appears as patches of the order of 2° to 3° in size, corresponding to 70–100 pc at the kinematic distance of the H I regions (approximately 2 kpc). This leads to a density of thermal electrons of up to $n \approx 0.15$ cm^{-3} (assuming a filling-factor of unity). Using a (uniform) magnetic field strength of $2.2\,\mu$G (as adopted by Heiles 1996 for the Solar vicinity), this results in an RM of ≈ 20 rad m^{-2} or less, which will produce rotations of the polarisation angles of 10° or so at 2.7 GHz. It is unlikely that the average values of n exceed 0.15 cm^{-3} by a large factor, because of the total-power emission which would result. For example, increasing n by a factor of 10 would elevate the emission measures to ≈ 200 cm^{-6} pc (and to even higher values for filling-factors less than unity). Such emission measures would

be detectable in the total-power survey data, and show up as a better anticorrelation between the total-power and polarised intensity images.

If we assume, then, that $n \approx 0.15$ cm^{-3} is an average value across the telescope beam, and that variations in n within the beam area rise to maxima of several times this value, we expect variations in the rotation of the polarisation angles within the beam of the order of 30°. Although an order-of-magnitude estimate, this value is not sufficiently small for us to exclude H I-associated thermal electrons as a source of significant depolarisation, and hence as a possible mechanism for the production of the anticorrelation seen in Fig. 7.

Another mechanism for producing the anticorrelation between polarised emission and H I is "tangling" of magnetic fields. In this case, the magnetic field within the denser regions of H I is tangled by the turbulent motions of the gas, resulting in no coherent Faraday rotation within the beam and leading to depolarisation. Outside the denser regions of H I the magnetic field is more uniform, resulting in less beam depolarisation. We note that a similar "tangled field" idea has been suggested to account for the low degrees of polarisation observed coincident with the arms of external galaxies (Beck et al. 1996, 1998). Here, this mechanism would require the magnetic field to be tangled on scales $\lesssim 0\overset{\circ}{.}2$, which corresponds to $\lesssim 10$ pc at a distance of 2 kpc.

Of course, both mechanisms may play a significant role in depolarising the emission.

5.4.4. The quasi-periodic structure

Examination of the data shows the polarisation angles of the brightly polarised regions (which give rise to the quasi-periodic patterns in Fig. 6) to deviate typically up to $\pm 45^\circ$ from one extremum to the other. At a distance of 2 kpc, the distance between peaks of approximately 7° longitude corresponds to $\simeq 250$ pc. If we consider the rotation to occur over a similar distance (i.e. that the "depth" of the structures is approximately 250 pc also), then a maximum value of

$$\langle B_l \rangle \langle n \rangle \simeq 0.3\,\mu\text{G cm}^{-3} \quad (1)$$

is required to produce this rotation at a frequency of 2.7 GHz, where $\langle n \rangle$ and $\langle B_l \rangle$ are the mean thermal electron density and line-of-sight component of the magnetic field, respectively, within the Faraday rotating region.

The strength of the uniform component of the magnetic field adopted by Heiles (1996) for the Solar vicinity of $2.2\,\mu$G and the electron density model presented by Taylor & Cordes (1993) lead to a typical value of $\simeq 0.2\,\mu$G cm^{-3} for z equal to 150 pc. As we are looking predominantly along the Sagittarius arm, the uniform component of the field is predominantly oriented along the line of sight. Thus, the required amount of rotation of the polarisation vectors can be supplied by the magneto-ionic medium of the Sagittarius spiral arm; no special field or electron density enhancements are required.

Although no enhancements in field strength or thermal electron density appear to be needed to produce the required Faraday rotation, a particular field geometry is still required. Fig. 6 shows vectors to be oriented at both positive and negative position angles. If this behaviour is produced through the action of Faraday RMs of opposite sign, then alternations of the direction of the line-of-sight component of the magnetic field are needed. Based on the calculations above, the required strength of this alternating field component is $\approx 2\,\mu$G.

We again note that, at distances of approximately 2 kpc, these polarised features are several hundred pc in size. Reaching z heights of several hundred pc above and below the Sagittarius spiral arm, it is possible that these magnetic field structures are produced by a mechanism similar to the Parker instability (e.g. Parker 1966; Giz & Shu 1993).

5.4.5. Local Faraday rotation?

Whilst the bright, polarised emission seen over the longitude range of $45^\circ \gtrsim l \gtrsim 20^\circ$ is probably produced at distances of between 2.5 and 8 kpc, we have not established the distance at which the quasi-periodic angle structure (Fig. 6) is imposed. Magnetic fields exhibiting similar "wave-like" patterns are known on much smaller linear scales (e.g. the Taurus dark cloud complex, as investigated by Goodman et al. 1990). It is therefore possible that this structure in the polarisation angles is produced through the Faraday effects of a relatively local magnetic field feature.

However, if the variations in the polarisation angles were imposed at relatively local distances ($d \simeq 300$ pc, say), then the magnetic field structures would be of correspondingly smaller linear size. This implies a much smaller path length over which the polarisation angles must be rotated, requiring far larger values for the field strength and/or thermal electron density over the region of rotation. For example, at a distance of 300 pc, the path length for Faraday rotation shrinks by an order of magnitude. Hence, an order of magnitude increase in $\langle B_l \rangle \langle n \rangle$ over the value in Eq. 1 would be required to produce the observed rotation. It is difficult to see how such increases could come about.

Furthermore, we note from Fig. 6 that the polarisation angles at positive Galactic latitudes are not correlated with those at negative latitudes. If a local magnetic field feature of modest linear size was responsible for the structure in Fig. 6, it is likely that the angles would show some correlation.

6. Conclusions

Polarimetric data from the Effelsberg 2.695 GHz survey have been successfully reduced, extending the Junkes et al. (1987a) work to the latitude limit of the survey ($b = \pm 5^\circ$). These data represent a high quality survey of the polarimetric emission throughout much of the first Galactic quadrant. The images reveal a large amount of bright, polarised emission towards higher latitudes, including an intriguing series of patches of bright, polarised emission between longitudes of 20° and 45° which apparently originate from the Sagittarius spiral arm, between distances of approximately 2.5 and 8 kpc. This emission is then

depolarised as it passes through regions of denser H I which lie at distances of 2 to 2.5 kpc (a Faraday "screen"), producing an anticorrelation between polarised intensities and H I gas. The depolarisation can be attributed to either an increased density of thermal particles associated with the denser H I regions, or to a significantly more "tangled" magnetic field (on scale-sizes up to ≈ 10 pc) within the regions, or both.

The structured, quasi-periodic nature of the polarisation position-angles over this region of the Plane most likely results from a peculiar magnetic field geometry associated with the Sagittarius arm. With scale-sizes of several hundred pc, such magnetic field geometries may be produced by a mechanism similar to the Parker instability.

It would be of considerable interest to see if a similar anticorrelation exists between H I data and the bright, polarised emission over longitudes of $-20^\circ \geq l \geq -45^\circ$. However, no dataset comparable to that of the Dwingeloo H I observations exists over the southern Galactic Plane. The forthcoming narrow-band H I survey with the multi-beam system at Parkes will assist here (Haynes et al. 1999).

In addition to detailed correlations of the polarised and unpolarised emission, more detailed interpretive work will require polarimetric data at other (preferably higher) frequencies; such observations are currently in progress. In the future, we also hope to extend this work (using the observations of Fürst et al. 1990) to cover the entire longitude range of the Galactic Plane.

7. Data availability

Access to the published survey data, as FITS format maps, is available through the *World Wide Web* server at the Max-Planck-Institut für Radioastronomie. The URL for this site is:

`http://www.mpifr-bonn.mpg.de/survey.html`

Acknowledgements. Much of the data presented in this paper was reduced while ARD was a guest of the Max-Planck-Institut für Radioastronomie in Bonn. ARD expresses his appreciation and thanks to both Prof. Richard Wielebinski and his group, and the Max-Planck Gesellschaft for their support during this time. The authors also express their appreciation to E.M. Berkhuijsen for helpful discussions, suggestions and comments which have greatly improved the manuscript. ARD is an Alexander von Humboldt research Fellow and thanks the Stiftung for their support.

References

Baars J.W.M., Genzel R., Pauliny-Toth I.I.K., Witzel A., 1977, A&A 61, 99
Beck R., Brandenburg A., Moss D., Shukurov A., Sokoloff D., 1996, ARA&A 34, 153
Beck R., Berkhuijsen E.M., Hoernes P., 1998, A&AS 129, 329
Beuermann K., Kanbach G., Berkhuijsen E.M., 1985, A&A 153, 17
Brand J., Blitz L., 1993, A&A 275, 67
Burn B.J., 1966, MNRAS 133, 67
Duncan A.R., Stewart R.T., Haynes R.F., Jones K.L., 1995, MNRAS 277, 36
Duncan A.R., Haynes R.F., Jones K.L., Stewart R.T., 1997, MNRAS 291, 279
Duncan A.R., Haynes R.F., Reich W., Reich P., Gray A.D., 1998, MNRAS 299, 942
Emerson D.T., Gräve R., 1988, A&A 190, 353
Fürst E., Reich W., Reich P., Reif K., 1990, A&AS 85, 691
Giz A.T., Shu F.H., 1993, ApJ 404, 185
Goodman A.A., Bastien P., Myers P.C., Ménard F., 1990, ApJ 359, 363
Gray A.D., Landecker T.L., Dewdney P.E., et al., 1999, ApJ 514, 221
Hartman D., Burton W.B., 1997, The Leiden/Dwingeloo Survey of H I in the Galaxy. Cambridge University Press, Cambridge
Haslam C.G.T., 1974, A&AS 15, 333
Haynes R., Staveley-Smith L., Mebold U., et al., 1999, In: Proc. IAU Symp. 190, New Views of the Magellanic Clouds. ASP, San Francisco, in press
Heiles C., 1996, In: Roberge W.R., Whittet D.C.B. (eds.) Polarimetry of the Interstellar Medium. Conf. Ser. Vol. 97, ASP, San Francisco, p. 447
Junkes N., Fürst E., Reich W., 1987a, A&AS 69, 451
Junkes N., Fürst E., Reich W., 1987b, In: Beck R., Gräve R. (eds.) Interstellar Magnetic Fields. Springer, Berlin, p. 115
Junkes N., Fürst E., Reich W., 1990, In: Beck R., Kronberg P.P., Wielebinski R. (eds.) Proc. IAU Symp. 140, Galactic and Intergalactic Magnetic Fields. Kluwer, Dordrecht, p. 63
Killeen N.E.B., Bicknell G.V., Ekers R.D., 1986, ApJ 302, 306
Parker E.N., 1966, ApJ 145, 811
Reich W., Fürst E., Steffen P., Reif K., Haslam C.G.T., 1984, A&AS 58, 197
Reich W., Fürst E., Reich P., Reif K., 1990, A&AS 85, 633
Reynolds R.J., Tufte S.L., Kung D.T., McCullough P.R., Heiles C., 1995, ApJ 448, 715
Sofue Y., Reich W., 1979, A&AS 38, 251
Sokoloff D.D., Bykov A.A., Shukurov A., et al., 1998, MNRAS 299, 189
Tabara H., Inoue M., 1980, A&AS 39, 379
Taylor J.H., Cordes J.M., 1993, ApJ 411, 674
Vallée J.P., 1987, Fundamentals of Cosmic Physics 19, 1
Wardle J.F.C., Kronberg P.P., 1974, ApJ 194, 249
Wieringa M.H., de Bruyn A.G., Jansen D., Brouw W.N., Katgert P., 1993, A&A 268, 215